E17-2013-18

E. B. Dushanov [1,2], Kh. T. Kholmurodov [1,3],
K. Yasuoka [4], E. A. Krasavin [1,3]

A COMPARATIVE **MD** ANALYSIS OF THE STRUCTURAL AND DIFFUSION PROPERTIES OF FORMAMIDE/WATER AND ETHANOL/WATER MIXTURES ON TiO_2 AND Pt SURFACES

Submitted to the Proceedings of the 5th Japan–Russia International Workshop MSSMBS'12, September 9–12, 2013, Dubna, Russia

[1] Laboratory of Radiation Biology, JINR, Dubna, Russia
[2] Institute of Nuclear Physics, Ulugbek, Tashkent, Uzbekistan
[3] Dubna International University, Dubna, Russia
[4] Department of Mechanical Engineering, Keio University, Minato, Tokyo, Japan

Душанов Э. Б. и др. E17-2013-18

Сравнительный анализ структурных и диффузионных свойств
водных растворов формамида и этанола на поверхностях TiO_2 и Pt

Взаимодействие «формамид–поверхность» являлось одной из основных тем обсуждения на круглом столе Италия–Россия@Дубна конференции «Астробиология: новые тенденции идей и исследований», организованной в 2011 г. Компоненты нуклеиновых кислот, синтезируемых из формамида и их аналогов, обнаруживаемых в космической пыли, рассматриваются в качестве основных кандидатов для начальной стадии формирования биологических молекул, необходимых для функционирования жизни. Диоксид титана (TiO_2, анатаз), диоксид циркония (ZrO_2) и другие минералы могут служить в качестве матричных элементов для синтеза нуклеиновых кислот из формамида, сопровождаемых температурным и ультрафиолетовым воздействием. Экспериментальные данные по адсорбции формамида, полученные в условиях темновой адаптации при 300 K на поверхности (001) TiO_2, указывают на некоторое количество не реагировавшего формамида и воды в среде продуктов реакции (CO, H_2, NH_3, HCN). Эксперименты показывают, что присутствие воды оказывает существенное влияние на взаимодействие формамида с поверхностью TiO_2. В настоящей работе проведено молекулярно-динамическое (МД) моделирование процессов взаимодействия раствора формамид–вода с поверхностью TiO_2 (анатаз). На основании полученных результатов МД-моделирования выполнен сравнительный анализ структурных и диффузионных свойств систем формамид–вода/(TiO_2, Pt) и этанол–вода/(TiO_2, Pt) в интервале температур от 250 до 400 K.

Работа выполнена в Лаборатории радиационной биологии ОИЯИ.

Препринт Объединенного института ядерных исследований. Дубна, 2013

Dushanov E. B. et al. E17-2013-18

A Comparative MD Analysis of the Structural
and Diffusion Properties of Formamide/Water
and Ethanol/Water Mixtures on TiO_2 and Pt Surfaces

Formamide–surface interaction was one of the main discussion topics at the round table meeting of the conference Italia–Russia@Dubna «Astrobiology: New Ideas and Research Trends» (2011). The nucleic acid components synthesized by formamide and their cosmic dust analogs have been widely considered to be the best candidates with regard to the early stages of the formation of biological molecules needed for life. Titanium dioxide (TiO_2, anatase), zircon (ZrO_2), and other minerals could influence as matrix elements for synthesis of nucleic acid bases from formamide, which is followed by temperature and UV heating. In the dark conditions, the experimental data on formamide adsorption at 300 K over the (001) plane of TiO_2 indicate some amount of unreacted formamide and water among the reaction products (CO, H_2, NH_3, HCN). So far, some concentration of water and its involvement in formamide/TiO_2 interaction has been experimentally shown to be an important component of the process. In this paper, molecular dynamics (MD) simulation of interaction between a formamide–water solution and a TiO_2 (anatase) surface is performed. A comparative MD analysis is done of the formamide–water/(TiO_2, Pt) and ethanol–water/(TiO_2, Pt) systems in a temperature range from 250 to 400 K to compare their structural and diffusion properties.

The investigation has been performed at the Laboratory of Radiation Biology, JINR.

Preprint of the Joint Institute for Nuclear Research. Dubna, 2013

1. INTRODUCTION

The photoreaction and adsorption properties on surfaces, thermal decomposition, chemical transformation, and other properties of the formamide molecule are widely used to understand the origins of the formation of biological molecules (nucleosides, amino acids, DNA, monolayers, etc.) needed for life. The titanium dioxide (TiO_2) surface can act both as a template on which the accumulation of adsorbed molecules like formamide occurs through the concentration effect, and as a catalytic material that lowers the activation energy needed for the formation of intermediate products. Formamide contains the four elements (C, H, O, and N) most required for life and it is attractive as a potential prebiotic starting material for nucleobase synthesis. In the presence of catalysts (for example, TiO_2) and with moderate heating, formamide can pass surface energy barriers, yielding a complete set of nucleic bases and acyclonucleosides, and favoring both phosphorylations and transphosphorylations necessary for life. In the reaction mechanism, interaction with water seems to be an essential factor for the formamide molecule to function [1–5]. An important type of nucleoside base synthesis can be supposed to take place under UV light in the formamide reaction with a TiO_2 surface, which would underlie the crucial biological significance of this mineral in making compounds of life. In the dark conditions, the experimental data on formamide adsorption at 300 K over the (001) plane of TiO_2 indicate some amount of unreacted formamide and water among the reaction products (CO, H_2, NH_3, HCN). Thus, some concentration of water and its involvement in formamide–TiO_2 interaction was experimentally shown to be an important constituent. Besides nucleoside synthesis, formamide actively influnces *in situ* the hybridization of nucleotide, DNA, and RNA molecules [1–8].

Formamide (CH_3NO, hereinafter also as FM), also known as methanamide, is an amide derived from formic acid. It is a clear liquid which is miscible with water and has an ammonia-like odor. When heated strongly, FM decomposes to hydrogen cyanide (HCN) and water vapor. As a constituent, FM is also used for the cryopreservation of tissues and organs. In relation to the DNA and RNA molecules, some important formamide's properties can be outlined as follows. It stabilizes RNA in gel electrophoresis by deionizing RNA; in capillary electrophoresis, it is used for stabilizing single strands of denatured DNA. FM lowers the melting point of nucleic acids, so the strands separate more readily [6]. Theoretical investigations of the chemical transformations of FM, a molecule of prebiotic interest as a precursor for biomolecules, are conducted concerning the formation of small molecules including CO, NH_3, H_2O, HCN, HNC, H_2, HNCO, and HOCN [9]. The solvent, dehydration, adsorption, and decomposition properties of formamide on various surfaces were intensively studied in recent experimental papers [1, 2, 10–13]. Some of these experimental results are summarized and described in [14]. In [15], it is shown for the first time that guanine, adenine,

and hypoxanthine can be produced from formamide in a single model prebiotic reaction at lower temperatures than previously reported if FM is subjected to UV irradiation during heating; this observation relaxes the requirements for prebiotic purine nucleobase formation.

The aim of this work is to simulate the formamide–water (FM–W) and ethanol–water (ETH–W) interaction process on the TiO_2 (anatase) and Pt (platinum) surfaces and to estimate the possible activation energy barrier with the MD method. Molecular modeling was performed for the temperature range from $T = 250$ K to $T = 400$ K, and the diffusion and density profiles were established for the formamide (FM), ethanol (ETH) and water (W) molecules on the TiO_2 (anatase) and Pt (platinum) surfaces. In this regard, metal surfaces are often used in the synthesis and degradation of oxygen-containing compounds, such as alcohols, where carbon–carbon (C–C) and carbon–oxygen (C–O) bond formation and breakage are the elementary steps in this type of process, and the metal surface plays the primary role in the efficiency and selectivity of these steps [22]. Few researches were performed on ethanol–water (ETH–W) surface. In Ref. [16], the authors studied the structure behavior and diffusion properties for an ETH–W solution and investigated the concentration dependence of properties. Wang Yao-Chun et al. used MD simulation to investigate the behavior of pure water molecules, ethanol molecules, and ETH–W mixture with various weight fractions inside Au nanotubes [17]. D. J. Cooke et al. studied the interface between the $\{10\bar{1}4\}$ surface of calcite and pure ethanol, pure water, and 50:50 mixture (by amount) of water and ethanol [18]. Before, in series of works we performed on ETH–W/Pt system for studying the structural and diffusion behavior of both ETH and W molecules on the surface of Pt (111) [19–21]. Apart from experimental research, recent theoretical and simulation studies were mostly focused on the FM–W reaction process. Several modern theoretical and molecular dynamics (MD) studies of FM–W interactions should be mentioned in this respect [23, 24]. Nevertheless, to our best knowledge, little is known about the FM/TiO_2 surface interaction, and almost nothing has been reported on the FM–W/TiO_2 one. In this paper, using the MD simulation method, we aimed to make the first attempts to investigate the FM/TiO_2 surface interaction mechanism in detail on the atomic/molecular level. In the presence of water (W), we elucidate the structural, diffusional, and molecular concentration distribution effects. We consider water presence to be a stabilizing factor on the FM/TiO_2 surface interaction mechanism.

2. MODELS AND SIMULATION METHODOLOGY

2.1. Initial Configurations, Molecular Field Topologies. We have simulated four liquid systems (pure FM, pure ETH, and FM–W and ETH–W mixtures) interacting with the TiO_2 and Pt surfaces. The configuration snapshots and schematic

views of the modelled systems are isllustrated in Figs. 1 and 2, respectively. Both FM–W and ETH–W mixtures contain 50–50% molecules of FM, ETH and W liquids. The pure (FM, ETH) and aqueous (FM–W, ETH–W) densities vary in the interval of $\rho = 0.7 - 1.0$ g/cm^3. For example, the system with pure FM has 2304

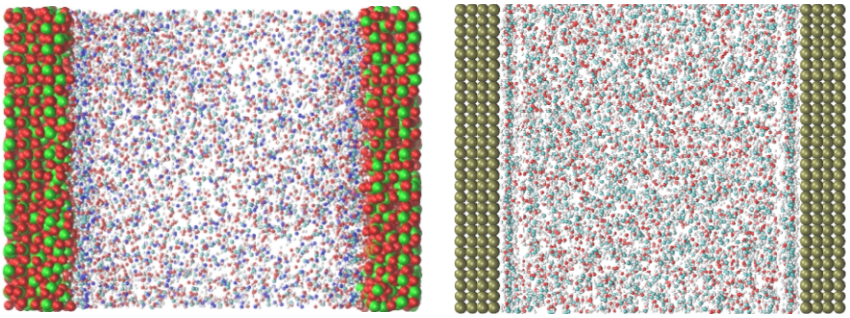

Fig. 1. (Color on-line). The computer generated snapshots of FM–W mixture relaxed in between two TiO_2 surface walls (left) and ETH–W mixture relaxed inside two Pt surface walls (right) are shown. The green and red large balls indicate Ti and O atoms, gray large balls — Pt atoms, small spheres — the FM–W and ETH–W liquid atoms, respectively

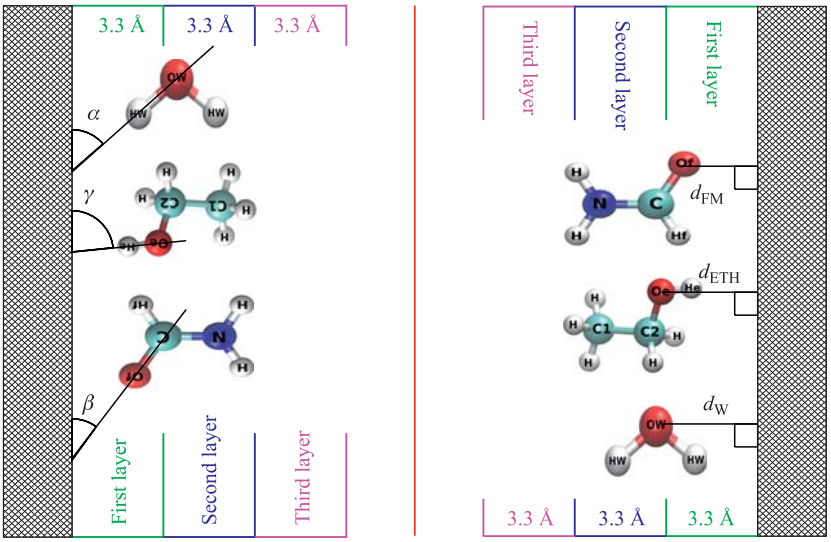

Fig. 2. A schematic view of the model systems. The FM molecules are shown as C, N, Of, Hf and H atomic sites; the ETH molecules — as C1, C2, Oe, He and H; the water — as OW and HW, respectively. The α, β and γ show the angles between the surfaces and the liquids OW–HW, C–Of and Oe–He bond distances. The d_{W}, d_{FM} and d_{ETH} display the minimal contact distances of the liquid oxygens to the surface planes

molecules, the FM–W system contains 1152 molecules of FM (formamide) and 1152 molecules of W (water). The ETH and ETH–W systems have also possess similar compositions as FM and FM–W ones. The bulk TiO_2 (anatase) phase was defined by the unit cell lattice vectors of following lengths: $a_0 = b_0 = 3.785$ Å and $c_0 = 9.514$ Å. The bulk Pt (platinum) phase was defined by the unit cell lattice vectors of the lengths: $a_0 = b_0 = c_0 = 3.923$ Å. All the lattice parameters of surface were taken from EIM databases supported by the Russian Foundation for Basic Research [25]. As for the adsorbing surfaces, we have composed totally four layers of 420 TiO_2 molecules (5040 = 1680 (Ti) + 3360 (O) atoms) and four layers of 784 Pt_4 molecules (3136 (Pt) atoms), respectively. The corresponding geometry parameters of the simulated systems are shown in Table 1.

Table 1. The details of the geometry and molecular compositions of simulated systems

System size	X, Å	Y, Å	Z, Å	ρ, g/cm^3	Ewald parameters (k_1, k_2, k_3)
$(TiO_2)_{5040}(CH_3NO)_{13824}$	56.77	52.99	73.06	1.06	22, 22, 30
$(Pt)_{3136}(CH_3NO)_{13824}$	54.99	54.99	69.22	1.06	22, 22, 28
$(TiO_2)_{5040}(H_2O)_{3456}(CH_3NO)_{6912}$	56.77	52.99	73.06	0.74	22, 22, 30
$(Pt)_{3136}(H_2O)_{3456}(CH_3NO)_{6912}$	54.99	54.99	69.22	0.74	22, 22, 28
$(TiO_2)_{5040}(C_2H_5OH)_{20736}$	56.77	52.99	72.56	1.09	22, 22, 30
$(Pt)_{3136}(C_2H_5OH)_{20736}$	54.92	54.92	69.22	1.09	22, 22, 28
$(TiO_2)_{5040}(H_2O)_{3456}(C_2H_5OH)_{10368}$	56.77	52.99	72.56	0.76	22, 22, 30
$(Pt)_{3136}(H_2O)_{3456}(C_2H_5OH)_{10368}$	54.92	54.92	69.22	0.76	22, 22, 28

For describing of van der Waals interactions we used Lennard-Jones (LJ) potential, which is commonly in use for simulation of liquids. The LJ and electrostatics potentials look like:

$$U = \sum_{ij} \left[4\varepsilon_{ij} \left(\left(\frac{\sigma_{ij}}{r_{ij}} \right)^{12} - \left(\frac{\sigma_{ij}}{r_{ij}} \right)^{6} \right) + \frac{q_i q_j}{r_{ij}} \right]. \quad (1)$$

Here $\sigma_{ij}, \varepsilon_{ij}$ are LJ interaction parameters for ith and jth atoms; r_{ij} is interatomic distance; q_i, q_j are partial atomic charges. The LJ, atomic charges and cross-interaction parameters for the FM–W liquid atoms are summarized in Table 5. The cross-section interaction parameters were defined using the Lorentz–Berthelot mixing rule: $\sigma_{ij} = (\sigma_i + \sigma_j)/2, \varepsilon_{ij} = (\varepsilon_i \varepsilon_j)^{1/2}$.

The intramolecular interactions between the liquid molecules were described using the LJ, combined with harmonic, angular and dihedral bonding potentials. For the surface atoms we used the Buckingham [26] and quartic tethering interaction potentials. For the Pt surface, the Sutton–Chen potential [27] was used.

The force field models for the TiO_2 (anatase) surface was reported by Kavathekar et al. [28] and Guillot et al. [29]. For the TiO_2 surface models,

the potential parameters were developed by Matsui and Akaogi [26]. The pair potential parameters from [30] were used to approximate the Pt–N interaction.

For water, the SPC rigid body model was used [31–33], and the water bond angles and lengths were not constrained.

2.2. Ensemble, Integration Algorithm, Force Fields. A classical molecular dynamics study was performed using the DL_POLY_2.20 [34] general-purpose code. The NVT ensemble with a Nosé–Hoover thermostat and a Verlet leapfrog scheme were employed. To calculate the long-range electrostatic forces, the three-dimensional Ewald summation with the automatic optimization parameter $f = 1.0 \cdot 10^{-4}$ and convergence parameter $\alpha = 0.24375$ Å^{-1} was used. The integration time step of the dynamical equations of motion was 1 fs.

For the FM (formamide), ETH (ethanol) and W (water) molecules, the force field parameters were choosen from the DL_FIELD database [35], which, in their turn, were taken from the CHARMM package database [36].

The detailed potential and force field topology parameters (chemical, angular, and dihedral bonds, the partial atomic charges, etc.) of FM and other components are described below in Tables 4–6.

A parallel Shake algorithm expressed in terms of the replicated data strategy for constraining the rigid and other chemical bonds was used [34].

The MD simulations were realized in the temperature range from 250 up to 400 K with a step of $\Delta T = 25$ K.

3. RESULTS AND DISCUSSIONS

We generated the molecular dynamical trajectories and found the relaxed molecular configuration states for the large atomic ensembles that simulate the pure FM and FM–W mixture interacting with TiO_2 (anatase) surface. The FM/TiO_2 and FM–W/TiO_2 interaction processes were performed within the temperature range of 250–400 K. Next, we repeated the simulations to generate the FM–W interaction on a Pt (platinum) surface, as like as for FM–W/TiO_2 system. Finally, for the sake of comparative analysis, the above procedure have been fulfilled to simulate the ETH–W mixture on the same surfaces (TiO_2, Pt) under similar environmental and thermodynamical parameters.

3.1. Z-Density, Dipole Angle Orientations and Diffusion Coefficients. ***3.1.1. The density profiles and dipole angle orientations.*** The Z-density distributions of the FM and ETH oxygens (Of and Oe atoms), perpendicular to the TiO_2 and Pt surface planes, are shown in Fig. 3, *a*, *b*. Figure 3, *a* compares the Z-densities of pure FM (dashed curve) and FM–W mixture (solid line); Fig. 3, *b* — the Z-densities of pure ETH (dashed curve) and ETH–W mixture (solid line), respectively. Separately, in the same Fig. 3, *a*, *b*, the Z-density distributions of water oxygen (OW atom) are presented for the FM–W and ETH–W mixtures, respec-

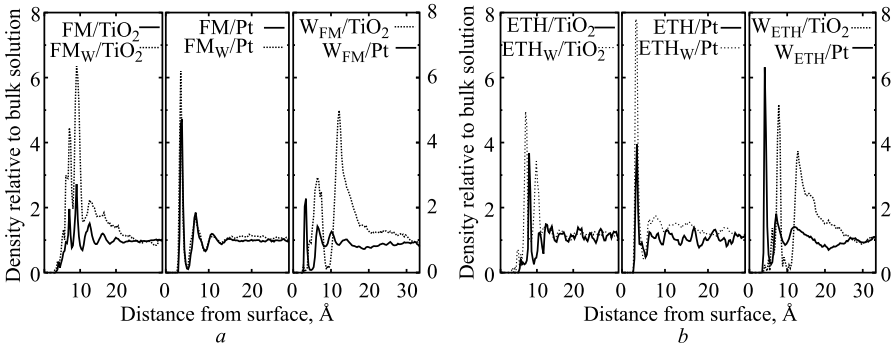

Fig. 3. The Z-density distributions of FM, FM–W (*a*) and ETH, ETH–W (*b*) solutions on TiO_2 and Pt surfaces

tively. The comparison of the results in Fig. 3, *a*, *b* indicates that the inclusion of water into consideration has to bring a substantial enhance of the FM and ETH density distributions in normal direction to the surface planes. On TiO_2 surface the Z-density amplitudes between the pure FM and FM in FM–W mixture have to differ more than twice; on Pt surface the amplitudes have not much differ from each other. The Z-density amplitudes between the pure ETH and ET in ETH–W mixture also differ exactly two times, but it happens on the Pt surface; on TiO_2 surface the amplitudes are close to each other.

Next, we introduced three distances, d_{FM}, d_{ETH}, and d_{W} to estimate the minimal contacts between the surface Ti and Pt atoms and the liquid oxygens (Of, Oe, and OW). The calculation results for the minimal surface–liquid distances are summarized in Table 2. As is seen, the minimal contact Ti–Of distance has to be equal to $d_{\mathrm{FM}} = 2.863$ Å in absence of water, and equal to $d_{\mathrm{FM}} = 2.783$ Å in the presence of water. For water on TiO_2 surface we have obtained that the minimal Ti–OW distance is equal to $d_{\mathrm{W}} = 2.383$ Å.

Table 2. Minimal surface–liquid distances (Å)

Surface	d_{FM}	$d_{\mathrm{FM}}(\mathrm{W})$	$d_W(\mathrm{FM})$	d_{ETH}	$d_{\mathrm{ETH}}(\mathrm{W})$	$d_{\mathrm{W}}(\mathrm{ETH})$
TiO_2	2.863	2.783	2.383	2.639	2.646	2.389
Pt	2.599	2.517	2.518	2.568	2.585	2.580

Next, for all simulated models, (FM, ETH, FM–W, ETH–W)/(TiO_2, Pt), the angles between the TiO_2 and Pt surface planes and the liquid atomic pair bonds (C–Of and Oe–He) were calculated. The liquid area was divided into three equal intervals, each of about 3.3 Å width, and the angles between the liquid bonds and the normal to the surface planes were estimated. Figure 2 displays the FM–W and ETH–W liquid layers, embedded between two TiO_2 and Pt wall surfaces. The calculation results of the dipole bond distribution are presented in Table 3.

Table 3. The dipole angle orientations on the TiO_2 and Pt surface walls (%)

	Anatase surface						Platinum surface					
Ang.\ Bond	C–Of	C–Of	OW–HW	Oe–He	Oe–He	OW–HW	C–Of	C–Of	OW–HW	Oe–He	Oe–He	OW–HW
First layer (thickness 3.3 Å, distance from surface 0 Å)												
30					24.0							
40				42.0	49.0							
50				57.0	24.5						0.50	
60		0.50		01.0	02.5						16.5	
70	06.0	34.5							11.5		45.0	05.0
80	91.0	65.0				01.5	01.0	06.5	45.5	02.0	33.5	38.5
90	03.0					13.5	48.0	54.5	38.0	81.5	04.5	53.0
100			06.0			31.5	49.5	39.0	05.0	16.5		03.5
110			49.0			34.0	01.5					
120			39.5			17.0						
130			05.5			02.5						
Second layer (thickness 3.3 Å, distance from surface 3.3 Å)												
50					46.0							
60				0.50	51.5							
70				32.5	02.5		02.0	01.5			02.5	01.0
80			26.0	61.5		18.0	70.5	45.5	13.0		29.0	20.5
90			57.5	05.5		58.0	27.5	50.0	60.5	06.0	52.5	45.0
100	55.0	46.5	16.5			23.0		03.0	26.5	82.0	16.0	29.5
110	45.0	53.5				01.0				12.0		04.0
Third layer (thickness 3.3 Å, distance from surface 6.6 Å)												
70			06.0	37.0		02.5	0.50	01.5			02.5	
80		01.5	57.5	62.0	03.5	49.0	12.0	29.0	23.0	30.5	27.0	14.5
90	0.50	26.5	36.0	01.0	33.5	45.0	76.5	55.0	57.5	69.5	54.5	64.5
100	49.0	58.0	0.50		54.5	03.5	11.0	14.5	18.0		15.5	21.0
110	49.5	14.0			08.5				01.5		0.50	

In the first layer, the C–Of bonds of pure formamide on TiO_2 surface are mostly oriented under 80° (91.0%). For the formamide with water, the most percentage of the C–Of bonds (65%) in the first layer are oriented under 80° relative to the surface plane. At the same time, the water bonds are being oriented from 110 to 120° (comparing the 4th column with 2nd and 3rd ones in Table 3). The Oe–He bonds of pure ethanol on TiO_2 surface are mostly oriented in 40–50° (the percentage varies between 42.0% and 57.0%, respectively). For the ethanol with water, the most percentage of the Oe–He bonds (49%) in the first layer are oriented under 40° to the surface. The water bonds of the ETH–W mixture are oriented from 90 to 120° (compare the 7th column with 5th and 6th ones in Table 3). The C–Of bonds of pure FM and FM–W mixture on Pt surface are mostly oriented under 90–100° (the percentage varies between 48.0–49.5% and 54.5–39.0%, respectively). The water OW–HW bonds for both FM–W and

ETH–W mixtures are oriented under 90° (compare the 10th and 13th columns with 7th, 8th, 11th and 12th ones in Table 3). The Oe–He bonds of pure ethanol are oriented under 90° (81.5%). For the ETH with water, the most percentage of the liquid bonds (45%) are oriented under 70° relative to the surface.

On the second layer, the C–Of dipole angles of both FM and FM–W mixtures are oriented under 100 and 110° to the TiO_2 surface plane, and under 80 and 90° to the Pt surface plane (Table 3).

In the third layer, the C–Of bonds of pure formamide are directed under 100 and 110° (the percentage are 49 and 49.5%, respectively); for the formamide with water, the C–Of bonds are oriented around 10° (the percentage is 58.0%).

It is worth noting that the dipole orientations as shown in Table 3 are in good agreement with the Z-density distributions presented in Fig. 3, *a*, *b*. From Fig. 3, *a*, *b*, one can observe that the Z-density amplitudes of both pure formamide (FM) and formamide with water (FM_W) are located on the same distance from the surface plane (6.6 to 9.9 Å), where the second and third layers are positioned. However, the inclusion of water into models substantially influences both the dipole angles and Z-density distributions. The Z-density amplitude of formamide in water is twice larger than for pure formamide, thereby originating from the dipole angle orientations. The comparison of results in Fig. 3, *a*, *b* and Table 3 are straightforward.

3.1.2. Diffusion coefficients. In this section, we investigate the behavior of important self-diffusion coefficient D for the ensembles of the FM, ETH, and W molecules. The temperature of the system was varied, and the effect of the temperature changes on the self-diffusion coefficients of the FM, ETH, and W molecules were estimated. Figure 4, *a* presents the values of D for the FM and FM–W mixture, Fig. 4, *b* — for the ETH and ETH–W mixture interacting with the TiO_2 and Pt surfaces, respectively. The diffusion coefficients decrease with temperature decreasing, which is consistent with the formation of longer H-bonded chains at low temperatures. The presence of the surfaces at low temperatures (275–290 K) has no effect on the value of D for all (FM, ETH, and W) liquids.

Let us compare the values of the diffusion coefficient D, estimated on TiO_2 (anatase) and Pt surfaces for 50:50% FM–W solution at 300 K, with experimental and other MD simulations of data (in [37, 38], etc.). There is seen the lack of experimental and simulation data regarding on the (FM–W, ETH–W)/(TiO_2, Pt) systems, so we compared our data with those existing in the experiment or in other simulations, but without any surfaces. From [37], the diffusion coefficient of the FM molecules was about $0.85 \cdot 10^{-9}$ m^2s^{-1} (experimental data for the FM–W mixture (no adsorbing surfaces). From our MD results, we obtain that the value of D_f to be around $0.997 \cdot 10^{-9}$ m^2s^{-1} and $1.317 \cdot 10^{-9}$ m^2s^{-1} correspondingly to TiO_2 and Pt surfaces. Thus, the presence of the surfaces has to reestimate the experimental value to about 17.3% (TiO_2) and 54.9% (Pt), respectively. At the same time, the self-diffusion coefficient of water (in FM–W) on TiO_2 and

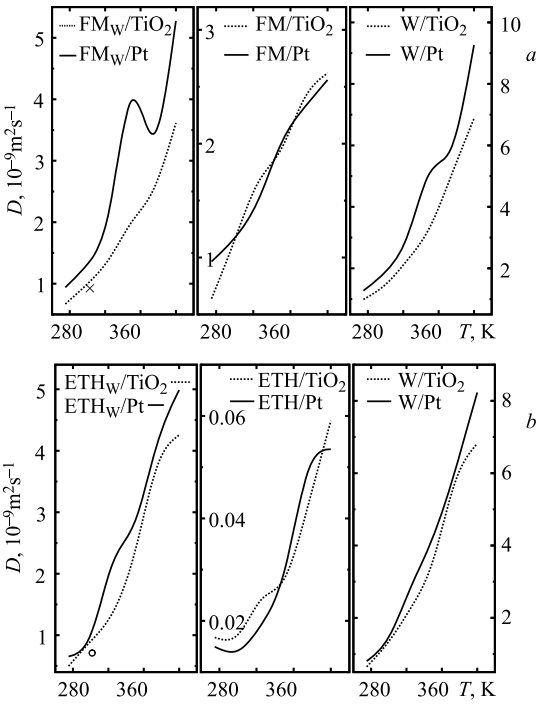

Fig. 4. Self-diffusion coefficients for FM and FM–W mixture and W (*a*) and for ETH and ETH–W mixture and W (*b*) as a function of temperature. The × is experimental data taken from [37, 38]. The ○ is experimental data taken from [16]

Pt surfaces have $1.474 \cdot 10^{-9}$ m^{2}s^{-1} and $1.889 \cdot 10^{-9}$ m^{2}s^{-1}, respectively. The latter D values are also higher than the data obtained in [38]: $1.35 \cdot 10^{-9}$ m^{2}s^{-1} (without surface).

The diffusion coefficient estimated for a 50:50% ETH–W solution at 300 K on TiO_2 (anatase) and Pt surfaces were also compared with the experimental and simulation data (in [16], etc.). The diffusion coefficient of the ETH molecules from [16] was about $0.7 \cdot 10^{-9}$ m^{2}s^{-1} (experimental data for the ETH–W mixture but without any surfaces). From our results, we obtain that the D_e values to be around $0.901 \cdot 10^{-9}$ m^{2}s^{-1} and $1.01 \cdot 10^{-9}$ m^{2}s^{-1} correspondingly to TiO_2 and Pt surfaces. So far, the presence of the adsorbing surfaces has to reestimate the existing experimental results to about 28.7 and 44.3% corrections. At the same time, for water (in ETH–W), the self-diffusion coefficients are of about $1.348 \cdot 10^{-9}$ m^{2}s^{-1} and $1.471 \cdot 10^{-9}$ m^{2}s^{-1} on TiO_2 and Pt surfaces, which are also higher than the experimental $0.88 \cdot 10^{-9}$ m^{2}s^{-1} ones.

3.2. Peculiarities of Structure Formations. Hereinafter, Hf, HW, Of, and OW denote, respectively, the hydrogen atoms of formamide and water and oxygen atoms of formamide and water.

3.2.1. Liquid–surface ordering. The structure of liquids generally is expressed in terms of the radial distribution functions (RDFs) $g(r)$. The most structured and interesting $g(r)$ functions for the liquid like a FM–W solution correspond to the oxygen–oxygen and oxygen–hydrogen bondings. Figure 5 shows the structural arrangement of FM–W system on TiO_2 and Pt surfaces. Figure 5 demonstrates the peculiarities of the RDF graphs of the Of–Of, OW–OW, Of–HW, and OW–Hf atomic pairs in a formamide–water mixture. It is seen that

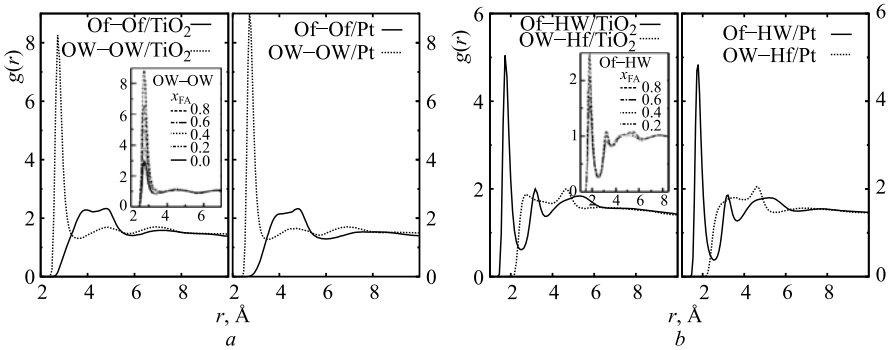

Fig. 5. The FM–FM, W–W and FM–W radial distribution functions (RDFs) $g(r)$ are shown. The $g(r)$ represent the Of–Of, OW–OW (*a*), Of–HW and OW–Hf (*b*) atomic pair ordering. Subpictures show the RDFs for the OW–OW and Of–HW atomic pair interactions in the absence of surface taken from [38]

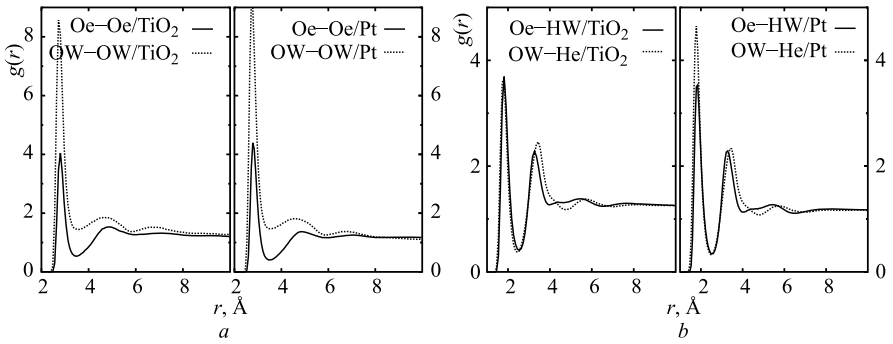

Fig. 6. The ETH–ETH, W–W and ETH–W radial distribution functions (RDFs) $g(r)$ are shown. The $g(r)$ represent the Oe–Oe, OW–OW (*a*), Oe–HW and OW–He (*b*) atomic pair ordering

the behavior of the RDF for water oxygen (OW–OW) is more ordered than that of (Of–Of) one. The first RDF g[OW–OW] peak is located at 3 Å from the zero point, which is 1.5 Å shorter than the g[Of–Of] one. At the same time, the Of–HW interaction looks much stronger than that of the OW–Hf atomic pair. The amplitude of the first g[Of–HW] RDF peak is located at 2 Å and it is twice higher than that of g[OW–Hf]. The peak of the g[OW–Hf] is located at 2.8 Å.

We also built the RDF $g(r)$ functions for a ETH–W liquid like a FM–W one with regard to the oxygen–oxygen and oxygen–hydrogen bondings. Hereinafter, He, HW, Oe, and OW denote, respectively, the hydrogen atoms of ethanol and water; and oxygen atoms of ethanol and water. Figure 6 shows the ETH–W/(TiO_2, Pt) structural arrangement, the peculiarities of the RDF graphs of the Oe–Oe, OW–OW, Oe–HW, and OW–He atomic pairs in the ethanol–water mixture. It is seen that the behavior of the RDF curves for water oxygens (OW–OW) is the same as for ethanol oxygens (Oe–Oe) one. However, the OW–OW pair shows more stronger ordering, as the amplitudes of the g[OW–OW] are much higher in comparison to g[Oe–Oe] ones (Fig. 6, a). The first RDF g[OW–OW]

Table 4. The force field potentials and parameters for TiO_2 and Pt surfaces

Buckingham potential for TiO_2: $A_{ij}\exp(-r_{ij}/\rho_{ij}) - C_{ij}/r_{ij}^6$					
$i-j$	A_{ij} (kcal mol^{-1})	ρ (Å)	C_{ij} (kcal mol^{-1} Å^6)		
Ti–Ti	717647.4	0.154	121.067		
Ti–O	391049.1	0.194	290.331		
O–O	271716.3	0.234	696.888		
Quartic tethering potential parameters for Pt and TiO_2: $kr^2/2 + k'r^3/3 + k''r^4/4$					
k, kcal mol^{-1}/Å^2		k', kcal mol^{-1}/Å^3		k'', kcal mol^{-1}/Å^4	
0.4		0.0		0.4	
Sutton–Chen potential parameters for Pt: $\varepsilon[\sum_j (a/r_{ij})^N/2 - C\sqrt{\rho_i}], \rho_i = \sum_j (a/r_{ij})^M$					
ε, kcal mol^{-1}	a, Å	N	M	C	
0.226	3.92	11.0	7.0	71.336	

Table 5. LJ parameters and charges of solution atoms and cross-interaction parameters for liquid–surface

Ethanol				Formamide				Liquid–Surface		
Atom	ε, kcal/mol	σ, Å	q/e, p.c.	Atom	ε, kcal/mol	σ, Å	q/e, p.c.	$i-j$	ε, kcal/mol	σ, Å
C1	0.0800	3.6705	−0.27	N	0.2000	3.2963	−0.69	Ti–O	7.7253	2.3431
C2	0.0550	3.8754	+0.05	C	0.0700	3.5636	+0.42	Pt–O	0.9200	2.7000
Oe	0.1521	3.1538	−0.66	Of	0.1200	3.0291	−0.51	Ti–C	7.2630	4.1340
He	0.0460	0.4000	+0.43	Hf	0.0220	2.3520	+0.08	Pt–C	0.9400	2.9000
H	0.0220	2.3520	+0.09	H	0.0460	0.4000	+0.35	Ti–N	0.7010	4.1310
OW	0.1521	3.1506	−0.82	HW	0.0460	0.4000	+0.41	Pt–N	1.7687	3.0615

Table 6. The potential force field parameters for formamide and ethanol molecules

Harmonic bond potential: $K(r_{ij} - r_0)^2/2$					
Bond	K, Å·kcal/mol	r_0, Å	Bond	K, kcal mol^{-1}Å	r_0, Å
1–2	960.00	1.00	1–5	222.00	1.52
1–4	860.00	1.36	1–2	309.00	1.11
4–6	1300.00	1.23	5–6	309.00	1.11
4–5	634.26	1.10	5–8	428.00	1.42
1–6	100.00	2.37	8–9	545.00	0.94
1–5	100.00	1.98	1–3	309.00	1.11
1–3	960.00	1.00	1–4	309.00	1.11
			5–7	309.00	1.11
Lennard–Jones bond potential: $4\varepsilon((\sigma/r_{ij})^{12} - (\sigma/r_{ij})^6)$					
Bond	ε, kcal/mol	σ, Å			
2–6	0.0743	1.4473			
2–5	0.0318	1.3760			
3–6	0.0743	1.4473			
3–5	0.0318	1.3760			
Angular potential: $K\ (\theta_{ijk} - \theta_0)^2/2$					
Group	K, kcal/(mol rad^2)	θ_0, °	Group	K, kcal/mol rad^{-2}	θ_0, °
2–1–3	46.00	120.00	2–1–3	35.50	109.44
2–1–4	100.00	120.00	6–5–7	35.50	120.00
1–4–6	150.00	122.00	2–1–5	34.60	109.46
1–4–5	88.00	111.00	1–5–8	75.70	109.00
6–4–5	88.00	122.00	1–5–6	34.60	108.89
2–1–4	46.00	120.00	5–8–9	57.50	109.50
3–1–4	100.00	120.00	6–5–8	45.90	108.89
Dihedral potentials: $K[1 + \cos(m\varphi_{ijkn} - \delta)]$				$K(\varphi_{ijkn} - \varphi_0)^2/2$	
Group	K, kcal/mol	δ, °	m	Group	K, kcal/mol	φ_0, °
2–1–4–6	1.40	180	2.00	2–1–5–8	0.16	180
2–1–4–5	1.40	180	2.00	2–1–5–6	0.16	–60
3–1–4–6	1.40	180	2.00	6–5–8–9	0.14	–60
3–1–4–5	1.40	180	2.00	1–5–8–9	1.30	180
				2–1–5–7	0.16	60
				3–1–5–6	0.16	180
				3–1–5–7	0.16	–60
				3–1–5–8	0.16	60
				4–1–5–6	0.16	60
				4–1–5–7	0.16	–180
				4–1–5–8	0.16	–60
				7–5–8–9	0.14	60

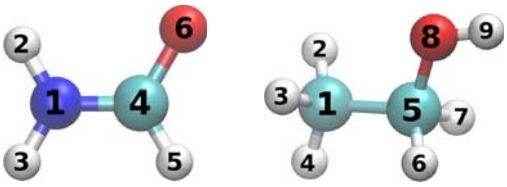

and g[Oe–Oe] peaks are located at 3 Å from the zero point. From Fig. 6, b for the RDF (OW–He) and (Oe–HW) one conclude that the Oe–HW interaction has a similar behavior as for OW–He atomic pair. The amplitude of the first RDF g[Oe–HW] peak is located at 2 Å.

3.2.2. Comparison with experiment (FM–W system). As was pointed out, there is a lack of experimental and simulation data for FM–W/TiO_2, so one compared our results with some experimental and other MD simulations, reported for the absence of the TiO_2 or Pt surface. In Fig. 5, the subpictures are taken from [38], where the RDFs for OW–OW and Of–HW pair interactions of the FM–W mixture were reported at the absence of surface. The comparision shows that the height of RDF picks are in agreement with the accuracy of 20%. It should be mentioned that in our FM–W system the FM ammount has a $\chi \approx 0.6$ mole fraction. Thus, the inclusion of TiO_2 (anatase) surface from our present study seems to essentially reestimate the structure formation in FM–W system.

4. CONCLUSIONS

Based on the molecular dynamics method and using the DL_POLY_2.20 code, we simulated the FM–W interaction process on a TiO_2 (anatase) surface. In the literature, we have noted the lack of experimental and MD simulation data on the FM–W/TiO_2 system. Our results were compared with the experimental and other MD simulation ones, which were performed in the absence of the surface. Our study shows that the inclusion of the TiO_2 (anatase) surface makes it necessary to reevaluate the structural and diffusion behavior of the FM–W system. The density distribution calculations were performed for the temperature range from 250 to 400 K. For pure formamide (FM), the density profile of FM/TiO_2 has a weak adsorption layer between two diffuse layers. The inclusion of water in the FM/TiO_2 model substantially changes the density distribution profiles normal to the surface; the amplitude of the density distribution for the FM–W/TiO_2 surface increases. Water strongly influences the FM diffusion capabilities on the surface. At the same time, comparing the structurally important radial distribution functions, we conclude that in the FM–W/TiO_2 interactions the water molecules actviley push formamide ones from the surface to the bulk area. Thus, including water in the system, one can see that it significantly influences both dynamical and structural behaviors of FM–W/TiO_2. A MD analysis of the formamide–water/(TiO_2, Pt) and ethanol–water/(TiO_2, Pt) systems has been performed for a temperature range from 250 to 400 K. A comparative analysis is performed of the FM–W/TiO_2 and FM–W/Pt and ethanol–water/(TiO_2, Pt) interactions. A MD analysis of the formamide–water/(TiO_2, Pt) and ethanol–water/(TiO_2, Pt) systems has been performed for a wide temperature range from 250 up to 400 K. There is a good agreement between the present MD simulation results and the experimental and

other simulation data on the structural, density and diffusion properties of the studied systems. The inclusion of the TiO_2 and Pt surfaces to the formamide–water and ethanol–water systems shows that their structural and diffusion properties have to be reevaluated. The reported data could stimulate further experiments in the field and might be useful for application purposes.

Acknowledgements. This work is a part of collaboration between JINR (Russia), RIKEN (Japan), and Keio University (Japan). The work has been performed within a research collaboration between JINR (Russia) and Keio University (Japan) and was jointly supported by the Japan Society for the Promotion of Science and the Russian Foundation for Basic Research (grant No.13-04-92100). The work has been supported in part by the Grant in Aid for the Global Center of Excellence Program to the Center for Education and Research of Symbiotic, Safe and Secure System Design from Japan's Ministry of Education, Culture, Sport, and Technology. The MD simulations have been performed using computer software, hardware facilities, and cluster machines at the CICC (JINR), RICC (RIKEN), and the Yasuoka Laboratory of Keio University (Japan). The authors would like to specially thank Sergei Negovelov (JINR) for technical assistance and helpful comments.

REFERENCES

1. *Senanayake S. D., Idriss H.* Photocatalysis and the Origin of Life: Synthesis of Nucleoside Bases from Formamide on TiO_2(001) Single Surfaces // Proc. of the National Academy of Sciences of the United States of America (PNAS). 2006. V. 103(5). P. 1194–1198.
2. *Saladino R., Crestini C., Costanzo G., Di Mauro E.* Advances in the Prebiotic Synthesis of Nucleic Acids Bases: Implications for the Origin of Life // Current Organic Chemistry. 2004. V. 8(15). P. 1425–1443.
3. *Ferris J. P., Hill A. R. (Jr.), Liu R., Orgel L. E.* Synthesis of Long Prebiotic Oligomers on Mineral Surfaces // Nature. 1996. V. 381(6577). P. 59–61.
4. *Ferris J. P.* Catalysis and Prebiotic RNA Synthesis // Origins of Life and Evolution of Biospheres. 1993. V. 23(5–6). P. 307–315.
5. *Huber C., Wächtershäuser G.* Peptides by Activation of Amino Acids with CO on (Ni, Fe)s Surfaces: Implications for the Origin of Life // Science. 1998. V. 281(5377). P. 670–672.
6. *Schoffstall A. M., Laing E. M.* Equilibration of Nucleotide Derivatives in Formamide // Origins of Life and Evolution of Biospheres. 1984. V. 14(1–4). P. 221–228.
7. *Schoffstall A. M., Barto R. J., Ramos D. L.* Nucleoside and Deoxynucleoside Phosphorylation in Formamide Solutions // Origins of Life and Evolution of Biospheres. 1982. V. 12(2). P. 143–151.

8. *Berndt A., Kosmehl H., Celeda D., Katenkamp D.* Reduced Formamide Content and Hybridization Temperature Results in Increased Non-Radioactive mRNA *in situ* Hybridization Signals // Acta Histochemica. 1996. V. 98(1). P. 79–87.
9. *Nguyen V. S. et al.* Theoretical Study of Formamide Decomposition Pathways // J. Phys. Chem. A. 2011. V. 115(5). P. 841–851.
10. *Kamineni V. K., Lvov Y. M., Dobbins T. A.* Layer-by-Layer Nanoassembly of Polyelectrolytes Using Formamide as the Working Medium // Langmuir. 2007. V. 23(14). P. 7423–7427.
11. *Parmeter J. E., Schwalke U., Weinberg W. H.* Interaction of Formamide with the ru(001) Surface // J. Am. Chem. Soc. 1988. V. 110(1). P. 53–62.
12. *Muir J. M. R., Idriss H.* Formamide Reactions on Rutile TiO_2(011) Surface // Surface Science. 2009. V. 603(19). P. 2986–2990.
13. *Saladino R. et al.* One-Pot TiO_2-Catalyzed Synthesis of Nucleic Bases and Acyclonucleosides from Formamide: Implications for the Origin of Life // ChemBioChem. 2003. V. 4(6). P. 514–521.
14. *Saladino R. et al.* Formamide Chemistry and the Origin of Informational Polymers // Chemistry & Biodiversity. 2007. V. 4(4). P. 694–720.
15. *Barks H. L. et al.* Guanine, Adenine, and Hypoxanthine Production in UV-Irradiated Formamide Solutions: Relaxation of the Requirements for Prebiotic Purine Nucleobase Formation // ChemBioChem. 2010. V. 11(9). P. 1240–1243.
16. *Zhang C., Yang X.* Molecular Dynamics Simulation of Ethanol/Water Mixtures for Structure and Diffusion Properties // Fluid Phase Equilibria. 2005. V. 231(1). P. 1–10.
17. *Wang Y.-C., Chen C., Ju S.-P.* Adsorption Mechanism and Dynamic Behavior of Water and Ethanol Molecules Inside Au Nanotubes // Chinese Journal of Catalysis. 2008. V. 29(11). P. 1099–1106.
18. *Cooke D. J. et al.* Interaction of Ethanol and Water with the $\{10\bar{1}4\}$ Surface of Calcite // Langmuir. 2010. V. 26(18). P. 14520–14529.
19. *Kholmurodov K. et al.* Molecular Dynamics Simulation of the Interaction of Ethanol–Water Mixture with a Pt Surface // Natural Science. 2011. V. 3(12). P. 1011–1021.
20. *Kholmurodov K. et al.* Molecular Dynamics Study of Ethanol Solvated by Water on the Pt (III) Surface // Chemical Physics. 2012. V. 402(0). P. 41–47.
21. *Kholmurodov K. et al.* Structural and Diffusional Study of Pure Ethanol and Water on Pt(III) Surface Using Molecular Dynamics Simulation // European Chemical Bulletin. 2013. V. 2(5). P. 247–254.
22. *Sachtler W. M. H., Ichikawa M.* Catalytic Site Requirements for Elementary Steps in Syngas Conversion to Oxygenates over Promoted Rhodium // J. Phys. Chem. 1986. V. 90(20). P. 4752–4758.
23. *Chalmet S., Ruiz-López M. S.* Molecular Dynamics Simulation of Formamide in Water Using Density Functional Theory and Classical Potentials // J. Chem. Phys. 1999. V. 111(3). P. 1117.
24. *Pomata M. H. H., Laria D., Skaf M. S., Elola M. D.* Molecular Dynamics Simulations of AOT–Water/Formamide Reverse Micelles: Structural and Dynamical Properties // J. Chem. Phys. 2008. V. 129(24). P. 244503.

25. WWW–MINCRYST. Crystallographic and Crystallochemical Database for Minerals and Their Structural Analogues. 2012. http://database.iem.ac.ru/mincryst/
26. *Matsui M., Akaogi M.* Molecular Dynamics Simulation of the Structural and Physical Properties of the Four Polymorphs of TiO_2 // Molecular Simulation. 1991. V. 6(4–6). P. 239–244.
27. *Sutton A. P., Chen J.* Long-Range Finnis–Sinclair Potentials // Philosophical Magazine Letters. 1990. V. 61(3). P. 139–146.
28. *Kavathekar R. S. et al.* Molecular Dynamics Study of Water in Contact with the TiO_2 Rutile-110, 100, 101, 001 and Anatase-101, 001 Surface // Molecular Physics. 2011. V. 109(13). P 1649–1656.
29. *Guillot B., Sator N.* A Computer Simulation Study of Natural Silicate Melts. Part I: Low Pressure Properties // Geochimica et Cosmochimica Acta. 2007. V. 71(5). P. 1249–1265.
30. *Li Zh., Drazer G.* Fluid Enhancement of Particle Transport in Nanochannels // Physics of Fluids. 2006. V. 18(11). P. 117102.
31. *Berendsen H. J. C., Grigera J. R., Straatsma T. P.* The Missing Term in Effective Pair Potentials // J. Phys. Chem. 1987. V. 91. P. 6269–6271.
32. *Robinson G. W., Singh S., Zhu S.-B., Evans M. W.* Water in Biology, Chemistry and Physics: Experimental Overviews and Computational Methodologies // World Scientific Series in Contemporary Chemical Physics. 1996. V. 9. P. 528.
33. *Kusalik P. G., Svishchev I. M.* The Spatial Structure in Liquid Water // Science. 1994. V. 265. P. 1219–1221.
34. *Forester T. R., Smith W.* Dl_POLY_2.0: A General-Purpose Parallel Molecular Dynamics Simulation Package // Journal of Molecular Graphics. 1996. V. 14(3). P. 136–141.
35. *Yong C. W.* Dl_FIELD — A Force Field and Model Development Tool for DL_POLY / Ed. R. Blake // CSE Frontiers. STFCs Computational Science and Engineering Department (CSED). Science and Technology Facilities Council, STFC Daresbury Laboratory. 2010. P. 38–40.
36. *Brooks B. R. et al.* CHARMM: The Biomolecular Simulation Program // J. Comp. Chem. 2009. V. 30(10). P. 1545–1614.
37. *Finter C. K., Hertz H. G.* NMR Relaxation Study of I− and Na+ Solvation Structure in Formamide (FA) and Preferential Solvation of These Ions in the Mixture FA/H_2O // Zeitschr. Phys. Chem. 1986. V. 148(1). P. 75–96.
38. *Elola M. D., Ladanyi B. M.* Computational Study of Structural and Dynamical Properties of Formamide–Water Mixtures // J. Chem. Phys. 2006. V. 125(184506). P. 13.

Received on February 26, 2013.

Корректор *Т. Е. Попеко*

Подписано в печать 22.04.2013.
Формат 60 × 90/16. Бумага офсетная. Печать офсетная.
Усл. печ. л. 1,18. Уч.-изд. л. 1,59. Тираж 250 экз. Заказ № 57966.

Издательский отдел Объединенного института ядерных исследований
141980, г. Дубна, Московская обл., ул. Жолио-Кюри, 6.
E-mail: publish@jinr.ru
www.jinr.ru/publish/